

# Effect of anisotropic characteristics on the mechanical behavior of asphalt concrete overlay

Lingyun YOU<sup>a</sup>, Zhanping YOU<sup>a\*</sup>, Kezhen YAN<sup>b</sup>

<sup>a</sup> Department of Civil and Environmental Engineering, Michigan Technological University, Houghton, MI 49931, USA

<sup>b</sup> College of Civil Engineering, Hunan University, Changsha 410082, China

\*Corresponding author. E-mail: [zyou@mtu.edu](mailto:zyou@mtu.edu)

© Higher Education Press and Springer-Verlag GmbH Germany, part of Springer Nature 2018

**ABSTRACT** Asphalt concrete (AC) overlays placed over old asphalt pavement have become an alternative to repairing and reinforcing pavements. The strength contributed by the AC overlay is strongly influenced by the anisotropic properties of the pavement material. This study was conducted to analyze the influence of anisotropy, modulus gradient properties, and the condition of the AC overlay and old pavement contact plane on the mechanical behaviors of AC overlays, as well as to quantify the influence of the degree of anisotropy on the mechanical behaviors of AC overlay by a sensitivity analysis (SA). The mechanical behaviors of the AC overlay were numerically obtained using the three-dimensional finite element method with the aid of ABAQUS, a commercial program. Variations in the AC overlay's modulus as a function of temperature as well as the contact state between the AC overlay and AC layer were considered. The SA is based on standardized regression coefficients method. Comparing the mechanical behavior in terms of surface deflection, stress, and strain of the anisotropy model against those corresponding to the isotropic model under static loads show that the anisotropic properties had greater effects on the mechanical behavior of the AC overlay. In addition, the maximum shear stress in the AC overlay was the most significant output parameter affected by the degree of anisotropy. Therefore, future research concerning the reinforcement and repair of pavements should consider the anisotropic properties of the pavement materials.

**KEYWORDS** asphalt concrete overlay, anisotropy, temperature gradients, modulus gradients, finite element simulation, sensitivity analysis

## 1 Introduction

Asphalt concrete (AC) overlays are commonly used for rehabilitating deteriorated pavements because this method is effective when repairing and reinforcing pavements. The comfortability and durability of repaired or reinforced pavements is most dependent on the mechanical performance of the AC overlay. The analytical and experimental research of the design and analysis of AC overlay pavements have been intensified in recent years [1–6]. Pavement materials are usually assumed to be isotropic and homogeneous when deformation, stress, and strain were calculated during prior research of the AC overlay pavement theory. For example, in order to investigate the effectiveness of the inner stress-absorbing composite

layers to control reflection cracking, the laboratory pavement sample with AC overlay was constructed and tested by Dempsey [2]. Khodaii et al. [3] documented the effects of geo-synthetic reinforcement on mitigating reflection cracking in the AC overlay. Wang [5] studied the effects of using reclaimed asphalt pavement (RAP) on the long-term performance of AC overlays. These results show that the presence of RAP, the choice of pre-overlay treatment method, and overlay thickness work dependently upon one another in producing the long-term performance strength of the mixture [4]. Many researchers also have found that the AC materials are anisotropy [7–10]. The anisotropic characteristic of AC materials has obvious effects on the mechanical behaviors of pavement. In comparison to the traditional elastically isotropic material model, the use of an elastically anisotropic model to describe the mechanical behaviors produces more reliable

results [9,11–13]. It is more important to consider these anisotropic characteristics when the mechanical response solution of those materials was derived. In addition, sensitivity analysis (SA) was usually used to define the effect of the input parameters on the uncertainty of the outputs. Basic SA study the variation in the outputs by changing one input parameter while holding other input parameters fixed. Besides, in the global SA, the effect of a parameter is defined by varying all the parameters at the same time [14–17]. Few studies have been on the SA of anisotropic properties, to identify the influence of anisotropic characteristic on the mechanical behaviors of pavement.

AC, particularly its course surface, exhibits vertical grading properties, primarily caused by temperature and age-related stiffness of the gradients [18–20]. The research of Nazarian and Alvarado [18] produced an interesting result, showing that the variation in modulus of AC with temperature is a very important aspect to consider during the analyzation and design of pavement. Therefore, to successfully analyze the mechanical behaviors of AC overlay pavement, modulus gradient properties at different depths should be strictly considered. Additionally, the condition of the inner layer boundary between the AC overlay and the old AC surface are widely accepted as important factors affecting pavement performance [21]. The condition of the boundaries between each layer of pavement structure is assumed to be completely continuous. Unfortunately, this testing assumption does not correspond to the real condition of test specimens during design analysis. Guo et al. [22] stated that deformation of the pavement surface depends on the friction coefficient and modulus and that the state of interlayer bonding also has an important effect on pavement deflection. Therefore, the boundary condition between the AC overlay and old AC layers is a critical factor to be considered during analysis of the mechanical behavior of pavement.

Based on this brief background, the goal of this research is to study the influence of anisotropy, modulus gradient properties, and the condition of the AC overlay and old pavement contact plane on the mechanical behaviors of asphalt pavements. In addition, in this paper, a comprehensive SA is also presented to identify the effect of anisotropic characteristics on the mechanical behaviors.

## 2 Transversely isotropic and gradient properties of AC modulus

### 2.1 Transversely isotropic characteristics of AC

AC is composed of differently shaped granular materials and its internal structure shows obvious anisotropic characteristics. These anisotropic properties are due mainly to the distribution, shape, orientation, degree of compac-

tion, void structure, etc. of the granular materials.

The transversely isotropic of AC are usually regarded as a special type of anisotropic, and it can be a good characterization for the feature of anisotropic [9,10,23,24]. The main parameters of transversely isotropic materials include vertical elastic modulus,  $E_v$ , on the vertical plane, horizontal elastic modulus,  $E_h$ , on the horizontal plane along the transverse direction, Poisson's ratio for the vertical and horizontal directions, and shear modulus,  $G$ , which is assumed to be the same over three orthogonal planes. We usually assume that Poisson's ratio is equal in all directions and, therefore, introduced the modulus ration (the ratio of horizontal elastic modulus to vertical elastic modulus, i.e.,  $\alpha = E_h/E_v = E_x/E_z = E_y/E_z$ ) in order to characterize the transverse isotropy of AC, as shown in Fig. 1. Masad et al. [25] first discovered that the transversely isotropic properties of AC were formed by the Superpave rotary compactor. Recall that Wang et al. [9] measured the degree of transverse isotropy of AC using the tri-axial test *in situ*, which was determined to be between 0.2 and 0.5. Through vertical and horizontal dynamic modulus testing, Motola and Uzan determined that the degree of transverse isotropy of AC is 0.4. Using indoor experimentation, Ju [27] found that the degree of transverse isotropy of AC-20 is 0.75 to 0.85.

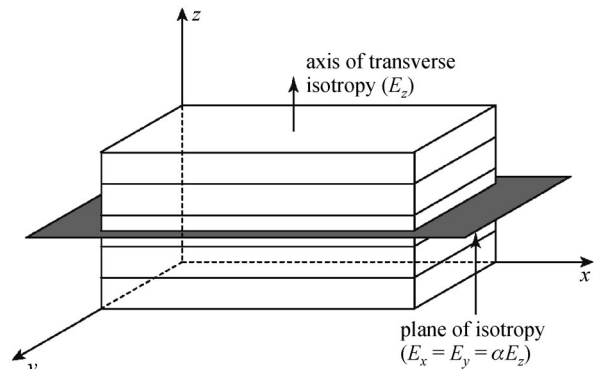


Fig. 1 Transverse isotropy characteristics

### 2.2 Modulus gradient properties of AC

AC is a material sensitive to temperature change; the road performance and mechanical properties of AC change significantly with temperature. Furthermore, at different depths within the pavement, the temperature varies in a district gradient pattern, also causing variation in the elastic modulus [18,28–30]. AC is a mixture of asphalt and mineral aggregate. The viscosity of asphalt increases sharply at low temperatures, which leads to the increase of cohesive force between aggregates. On the contrary, the viscosity of asphalt decreases sharply at high temperatures, which leads to the decrease of cohesive force between aggregates. As a result, the elastic modulus of AC

increases with decrease in temperature and decreases with increase in temperature [31].

A simple laboratory test of AC-20 is used in this study; the test method is comprehensively described in Refs. [32,33] and briefly discussed in this text. Variation in testing temperatures was considered to allow for the use of a larger variety of AC overlay pavement types in low temperature and high temperature environments. Flow time is defined as the time corresponding to the minimal rate of change of permanent axial strain during the tests conducted in this study. The static creep tri-axial test measures permanent deformation as a function of time when a constant load is applied to a cylindrical AC specimen. Lastly, cumulative permanent deformation is reported as a function of time during compression. This deformation has historically been categorized into three zones (primary, secondary and tertiary). The primary zone is characterized by a reduced rate of accumulated permanent deformation. Permanent strain accumulates in a relatively linear fashion in the secondary zone. The tertiary zone occurs as the specimen break and is characterized by a rise in accumulated permanent deformation [33–35]. In this study, a confined compression test was selected to replace the unconfined compression test for its more accurate simulation of reality. In this test, the deviator stress was 1380 kPa and the confining stress was 276 kPa [34]. For the static creep test, the low temperature (or high temperature) elastic modulus of AC was selected at a constant load time under different low temperature (or high temperature) conditions as shown in Fig. 2.

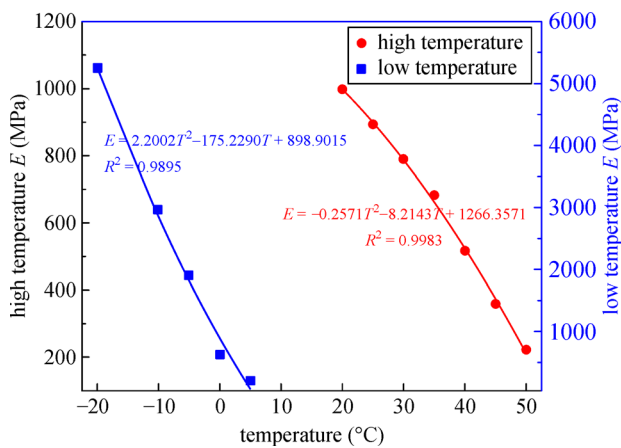


**Fig. 2** Test data of elastic modulus of asphalt concrete at different temperature condition

Results show that the low temperature elastic modulus of AC has a quadratic polynomial relationship with temperature. Correlation coefficient,  $R^2$ , is 0.9895. The relationship between the elastic modulus of low temperature testing conditions and the temperature ( $T$ ) of the material is shown in Eq. (1).

$$E = 2.2002T^2 - 175.2290T + 898.9015, \quad (1)$$

where  $E$  is elastic modulus and  $T$  is temperature.

Similarly, the relationship between the elastic modulus of high temperature and the temperature of the material is shown in Eq. (2). Correlation coefficient,  $R^2$ , is 0.9983.

$$E = -0.2571T^2 - 8.2143T + 1266.3571. \quad (2)$$

The temperature of AC material changes with the depth of the pavement structure due to the influence of many factors, such as atmospheric temperature, sun exposure, rainfall, frost, etc. The sun's effect on the temperature of AC at different depths of the pavement layer can be predicted using two (low temperature model and high temperature model) models. This process involves a large number of field measurements and statistical analysis [36]. The low temperature gradient model and high temperature gradient model are shown in Eqs. (3) and (4), respectively.

$$T_{\min} = \beta_1 + \beta_2 T_{a,\min} + \beta_3 H + \beta_4 H^2 + \beta_5 T_{m,\text{av}}, \quad (3)$$

where  $T_{\min}$  is the daily minimum temperature (°C) of the AC at depth  $H$ ,  $T_{a,\min}$  is the local daily minimum temperature (°C),  $H$  is the pavement depth (cm),  $T_{m,\text{av}}$  is the local monthly average temperature, and  $\beta_1$ – $\beta_5$  are the regression coefficients. For this study, experimental data, describing the low temperature performance of AC pavement, was obtained from Beijing. The average atmospheric temperature during data collection was  $-4.3$  °C and the daily minimum temperature, which occurred in January, was  $-15$  °C. The regression coefficients that appear in Eq. (3),  $\beta_1$ ,  $\beta_2$ ,  $\beta_3$ ,  $\beta_4$ , and  $\beta_5$ , are equal to  $-3.399$ ,  $0.721$ ,  $0.377$ ,  $0.010$ , and  $0.488$ , respectively.

$$T_{\max} = \gamma_1 + \gamma_2 T_{a,\max} + \gamma_3 T_{a,\max} H + \gamma_4 H + \gamma_5 H^2 + \gamma_6 H^3 + \gamma_7 T_{m,\text{av}}. \quad (4)$$

In Eq. (4),  $T_{\max}$  is the daily maximum temperature (°C) of the AC at depth  $H$ ,  $T_{a,\max}$  is the local daily maximum temperature (°C),  $H$  is the pavement depth (cm),  $T_{m,\text{av}}$  is the local monthly average temperature, and  $\gamma_1$ – $\gamma_7$  are the regression coefficients. Experimental data describing the high temperature performance of AC pavement was also collected in Beijing. The average atmospheric temperature during data collection was  $26.2$  °C and the daily maximum temperature, which occurred in July, was  $36$  °C. The regression coefficients that appear in Eq. (4),  $\gamma_1$ ,  $\gamma_2$ ,  $\gamma_3$ ,  $\gamma_4$ ,  $\gamma_5$ ,  $\gamma_6$ , and  $\gamma_7$ , are equal to  $3.04$ ,  $0.994$ ,  $-0.007$ ,  $-1.676$ ,  $0.201$ ,  $-0.008$ , and  $0.498$ , respectively.

Using Eqs. (1)–(4), the relationship between the elastic modulus of AC and the depth of the pavement structure at low and high temperatures can be described. This relationship is shown in Fig. 3.

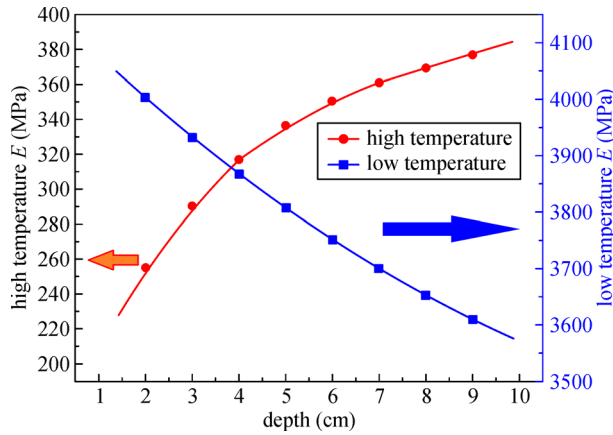


Fig. 3 Variation of elastic modulus of AC versus depth of pavement structure

### 3 FEM modeling in space and materials

#### 3.1 Finite element modeling of pavement structure and load

This section deals with the finite element modeling of the pavement structure. A three-dimensional (3D) model was developed using ABAQUS, version 6.14. In the finite element model, the eight-node, linear brick elements (C3D8R) were used to represent the finite domain of the pavement structure, and the infinite elements (CIN3D8) were used at model boundary to decrease the potential large number of far field elements without significant loss of accuracy [21]. The model, as shown in Fig. 4(a), had dimensions 10 m along the vertical  $z$  direction, 5 m along the lateral (or transverse)  $y$  direction, and 5 m along the

longitudinal  $x$  direction. This model consisted of four layers, with the top layer being the AC overlay with a thickness of 0.1 m, the second layer being the old AC layer with a thickness of 0.18 m, the third layer being the granular base layer with a thickness of 0.35 m, and the fourth (bottom) layer being the subgrade layer with a thickness of 9.37 m, a value far greater than that of the other structural layers [37–39].

The bonds between the AC overlay and old AC layer was relatively weak, generally being in a semi-smooth state. This type of interlayer contact was due to transmission stress; other layers fully bonded to each other due to long-term use. Actually, the contact between structural layers is a complex boundary of non-linearity, and contact area or pressure varies with external load [40]. To simulate the interlayer contact state between the AC overlay and old AC layer of pavement, the PENALTY function friction model was used. A non-embedding contact area is represented using the PENALTY function friction model which allows me to derive the penalty term, which is then used in the potential energy model. Thus, the contact problem is transmitted to the PENALTY function, where it can be solved using ABAQUS [40–42]. The interlayer friction coefficient was 0.5 when considering the low or high temperature modulus gradient. The effects of the interlayer boundary conditions on the mechanical behaviors of pavement were also discussed. Two types of interlayer boundary conditions were considered in this study. Firstly, the friction coefficients ( $f$ ) between the AC overlay and the old AC layer were 0.2 to 1.0, and the interlayer bonding state was nearly continuous when the friction coefficient equaled 1.0. Secondly, the interlayer interaction properties were set as bonding constrains

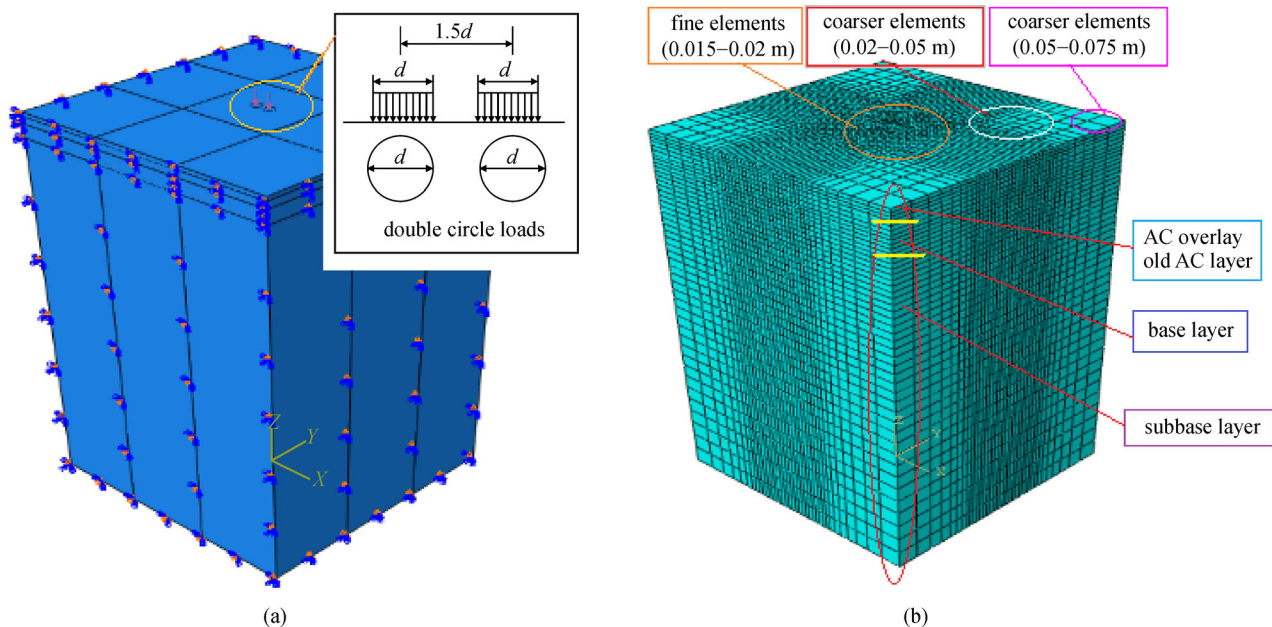


Fig. 4 Illustration of the developed 3D finite element modeling. (a) Boundary conditions and double circle loads; (b) element mesh

(pavement structure as a whole) when the AC overlay fully bonded to the old AC layer, represented by  $LX$  (a symbol used to characterize completely continuous) [43–45].

Figure 4(b) illustrates the mesh of the 3D finite element pavement model in a 3D view. The accuracy of stress was affected by the size of the mesh in the region where stress changed sharply. Therefore, the stress corresponding to different mesh densities should be calculated to investigate whether or not convergence was achieved. After completed this self-check work, fine mesh was used around the loading area ( $0.5\text{ m} \times 0.5\text{ m}$ ), while relatively coarser mesh was used as the distance to the load center increased in this study. Hence, the size of elements within the loading area was selected to be 0.015 to 0.02 m in the transverse and longitudinal directions. The element thicknesses were selected to be 0.02 m for the AC overlay and old AC layer, 0.02 to 0.05 m for the base layer, and 0.05 to 0.075 m for the subgrade layer. Coarser mesh was used as the depth increased [46–48].

The typical heavy vehicle, weighing 100 kN, used for the isotropic linear elastic analyses, was also used here in its distributed load form, which considered to be distributed over a symmetrical double circular area of a 213.0 mm diameter. The model's two loading circles are symmetric to the  $y$ - $z$  plane, and the distance between two centers of circles is  $1.5d$  ( $d$  is the diameter of the circle load area,  $1.5d = 319.5\text{ mm}$ ) at a magnitude of 0.7 MPa, as shown in Fig. 4(a) [47,49].

### 3.2 Modeling the material behavior of layers

This section briefly describes the transversely isotropic characteristic and modulus gradient properties of the pavement structure. The properties of the pavement layers used for the elastic analysis are shown in Table 1 [1,37,50–52].

To analyze the effects of transversely isotropic characteristic of AC (including the AC overlay and old AC layer) on the mechanical behaviors of pavement structure, transversely isotropic coefficients  $\alpha$  were considered to be 0.3, 0.5, 0.7, or 1.0 (isotropic) for AC materials (the vertical elastic modulus,  $E_v$ , is assumed to be fixed and the horizontal elastic modulus  $E_h = \alpha E_v$ ). This study also considers the idea that old AC deteriorates to a certain degree due to its long-term use and that the vertical modulus of elasticity of the old AC was reduced to a certain extent in this study ( $E_h = 1200\text{ MPa}$ ). In addition,

for investigation of the influence of the modulus gradient properties of AC (mainly for AC overlay) on the response of pavement, the relationship between the elastic modulus of AC and the depth of the pavement structure (as shown in Fig. 4) were used to perform the vertical elastic modulus of the AC overlay at different depths. The grade finite element of asphalt pavement was used in this study. The work of Buttlar et al. [29] contains an excellent discussion on this matter, which is also briefly described in this paper. Before using this method, a theoretical formulation for grade finite element method was provided followed by an implementation using the user material subroutine (UMAT) capability of the ABAQUS program. One advantage of this method is the ability to model modulus gradient properties of AC in a single pavement layer. One example of such properties is the stiffening effect caused by aging of the top layer of AC and modeling. Another advantage to using the aforementioned method is that modulus gradient between two conterminal layers can be modeled using a smooth transition of material properties, rather than a sharp transition as in the traditional method [18,29,53,54].

## 4 Numerical results and discussion

### 4.1 Analysis for the effects of low temperature modulus gradient

First, the effects of degree of AC transverse isotropy on the vertical surface deflection was investigated, which considered the low temperature modulus gradient of AC overlay. The distributions of surface deflection  $U_z$  on the AC overlay is plotted in Fig. 5. The results show that the surface deflection of the overlay decreased with the increase in distance to load center when the distance was greater than 0.16 m (from the center of circular loading area), and the maximum value appeared near the center of the circular loading area. Variation in surface deflection near the loading area was small. It should be noted that the value of the surface deflection increases slightly with the decrease in transversely isotropic coefficient  $\alpha$ . In comparison to the intermediate temperature condition ( $25\text{ }^\circ\text{C}$ ), the change in the surface deflection near the loading area was relatively slow, but the regions influenced by pavement structure deformation changed dramatically when the same load was applied. This fact has an important implication for the designing and analyzing asphalt

**Table 1** Geometry and materials of pavement

layer	elastic modulus (MPa)	Poisson's ratio	thickness (mm)	density ( $\text{kg/m}^3$ )
AC overlay	–	0.25	100	2400
old AC	$E_h = 1200\alpha$	0.25	180	2400
base	700	0.25	350	2300
subgrade	80	0.35	$\infty$	1800

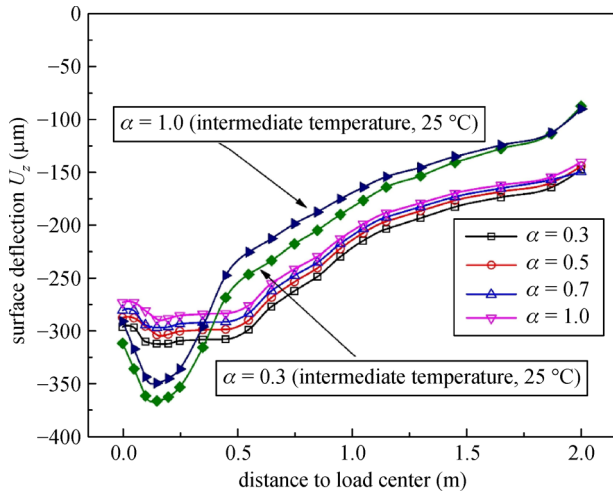


Fig. 5 Surface deflections at low temperature

pavement overlays. A larger surface deflection may imply that the level of rutting deformation might be underestimated by using isotropic elasticity analysis.

Secondly, the effect of transverse isotropy on the shear stress and shear strain at different depths of AC overlay were studied. Figures 6 and 7 show the relationship of the transversely isotropic coefficient,  $\alpha$ , with shear stress and shear strain at different depths, taking into consideration the low temperature modulus gradient of AC overlay. Figures 6 and 7 indicate that the shear stress and shear strain at the depth of about 3.0 cm near the maximum, under different degrees of transversely isotropic conditions ( $\alpha = 0.3, 0.5, 0.7, 1.0$ ), and the maximum shear stress/strain are 136.96 kPa/885.35  $\mu\epsilon$ , 144.89 kPa/936.56  $\mu\epsilon$ , 147.67 kPa/954.56  $\mu\epsilon$ , and 148.28 kPa/958.51  $\mu\epsilon$ , respectively. The shear stress and shear strain at the depth of 0 to 4.0 cm are great affected by the transversely isotropic coefficient,  $\alpha$  (shear stress and shear strain increased with the increase in the value of  $\alpha$ ), while it is only slightly affected by the

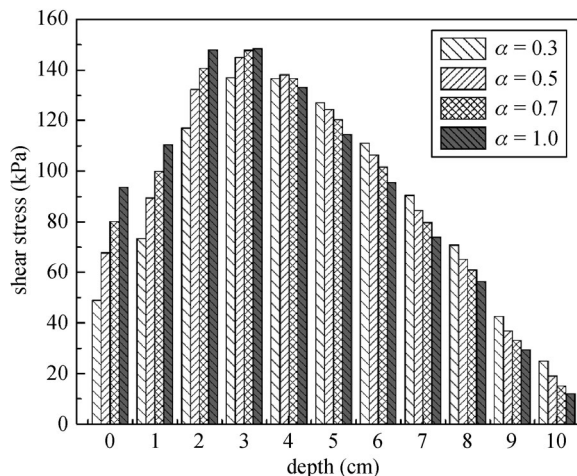


Fig. 6 Shear stresses of AC overlay at low temperature

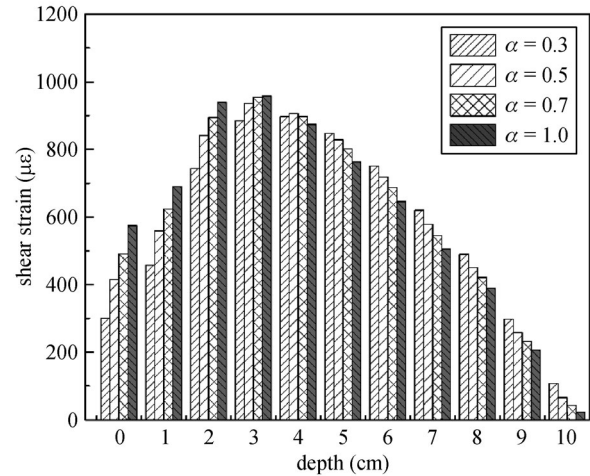


Fig. 7 Shear strains of AC overlay at low temperature

transversely isotropic coefficient  $\alpha$  at the depth of 4.0 to 10.0 cm (shear stress and shear strain decreased with the increase of  $\alpha$ ). At the same time, it can be seen from Figs. 6 and 7 that the peak value of shear stress and shear strain were obviously reduced with the decrease in the value of  $\alpha$ . The shear stress and shear strain at the depth of 4.0 to 10.0 cm under transversely isotropic conditions ( $\alpha = 0.3, 0.5, 0.7$ ) were greater than those of the isotropic condition. It is suggested that the shear stress and shear strain level might be underestimated by use of isotropic elasticity analysis.

#### 4.2 Analysis for the effects of high temperature modulus gradient

The relationship of transversely isotropic coefficients to the surface deflection with varying distances to the load center are presented in Fig. 8, which takes into consideration the high temperature modulus gradient of the AC overlay. Figure 8 shows that the surface deflection decreased with increase in the distance to the load center when the distance greater than 0.16 m (from the center of circular loading area). The maximum surface deflection value appeared near the center of the circular loading area; this changing trend near the loading area is very obvious. It should be noted that the peak value of surface deflection was smallest when the transversely isotropic coefficient,  $\alpha$ , equals to 0.3 ( $U_z = -611.60 \mu\text{m}$ ), and the crest of surface deflection was largest when the transversely isotropic coefficient  $\alpha$  equals to 1.0 (isotropic,  $U_z = -661.90 \mu\text{m}$ ). When the distance to the load center was more than 0.45 m, the surface deflection decreased with the increase of  $\alpha$ . The minimum surface deflection occurred when  $\alpha$  is equal to 1.0 (isotropy). In comparison to the intermediate temperature (25 °C), the surface deflection exhibited a steep increasing trend when considering the high temperature modulus gradient of AC overlay.

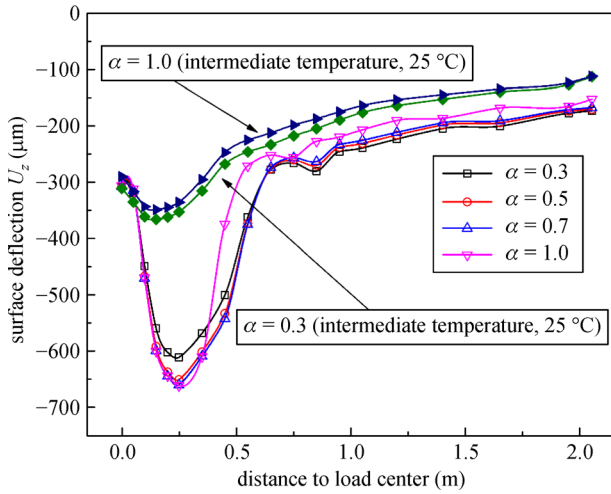


Fig. 8 Surface deflections at high temperature

Figures 9 and 10 demonstrate the relationships of transversely isotropic coefficient,  $\alpha$ , with shear stress and shear strain at different depths, taking into consideration the high temperature modulus gradient of AC overlay. Figures 9 and 10 indicate that the shear stress and shear strain occur at a depth of about 2.0 to 3.0 cm near the maximum under different transversely isotropic conditions ( $\alpha = 0.3, 0.5, 0.7, 1.0$ ). The shear stress and shear strain at a depth of 0 to 4.0 cm are greatly affected by the transversely isotropic coefficient (shear stress and shear strain increased with the increase in the value of  $\alpha$ ) while it is only slightly affected by transversely isotropic coefficient,  $\alpha$ , at the depth of 4.0 to 10.0 cm (shear stress and shear strain decreased with the increase of  $\alpha$ ). At the same time, it can be seen from Figs. 9 and 10 that the peak value of shear stress and shear strain were greatly reduced with the decrease of  $\alpha$ . The peak value of shear stress decreased by about 12% and the peak value of shear strain decreased by about 16%. A greater shear stress and shear strain at the

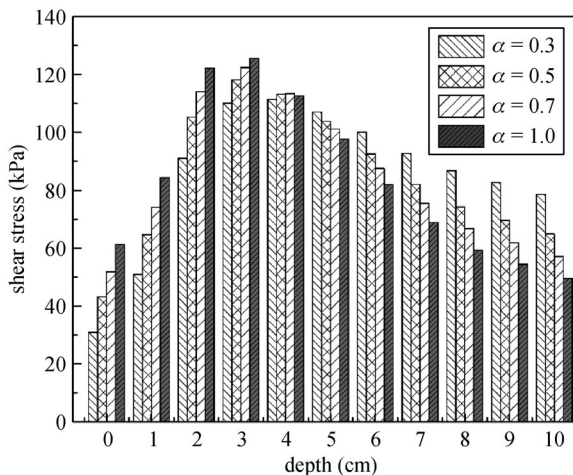


Fig. 9 Shear stresses of AC overlay at high temperature

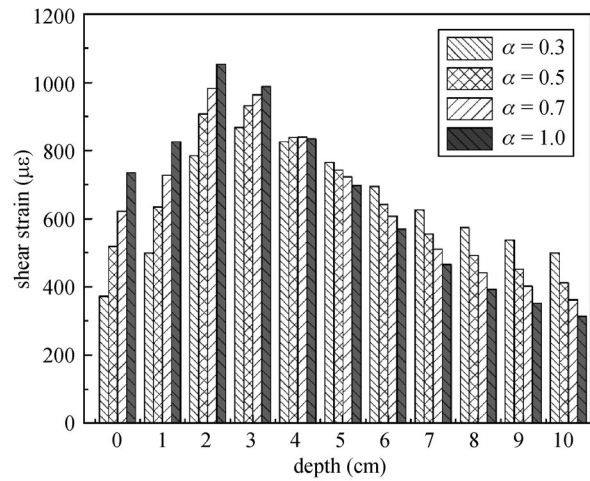


Fig. 10 Shear strains of AC overlay at high temperature

depth of 4.0 to 10.0 cm may imply that the shear stress and shear strain level for fatigue failure might be underestimated by using isotropic elasticity analysis.

4.3 Analysis for the effects of interlayer boundary condition

Figure 11 depicts the relationships between the maximum surface deflection and the interlayer bonding condition under different transversely isotropic conditions. We can see from Fig. 11 that the maximum surface deflection obviously increased with the degradation of the interlayer bonding condition (the interlayer friction coefficient,  $f$ , decreased). When full bonding,  $LX$ , had taken place, the surface deflection was less than that of a model with incomplete bonding. The surface deflection was larger as the degree of anisotropy of AC material enlarged (transversely isotropic coefficient,  $\alpha$ , decreased). When

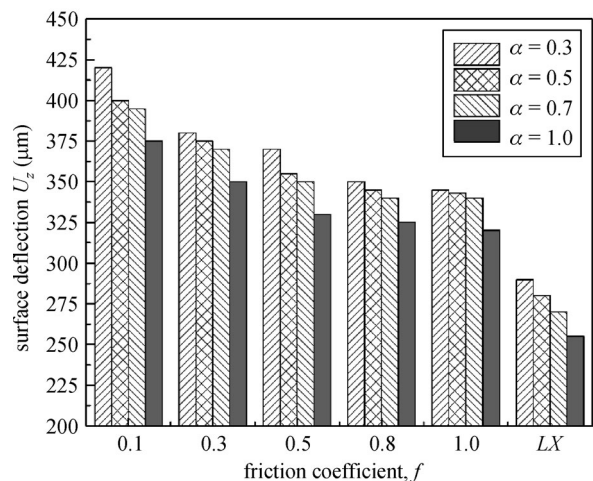


Fig. 11 Maximum surface deflection under different interlayer boundary condition (absolute value)

the value of  $f$  was equal to 0.1, the maximum surface deflection was  $421.55 \mu\text{m}$  when  $\alpha$  was equal to 0.3, while the maximum surface deflection was  $375.69 \mu\text{m}$  when  $\alpha$  was equal to 1.0. Under these conditions, isotropy reduced by nearly 11%. Figure 12 shows that the horizontal tensile strain at the bottom of the overlay was affected by the interlayer bonding condition as well as the transversely isotropic characteristic of AC. It is apparent that the tensile strain results decreased with respect to the interlayer bonding condition (the interlayer friction coefficient,  $f$ , increased). The friction coefficient,  $f$ , was equal to 1.0. The tensile horizontal tensile strain was equal to  $146.35 \mu\epsilon$  when  $\alpha$  was equal to 0.3, and when  $\alpha$  was equal to 1.0, the horizontal tensile strain was only  $63.38 \mu\epsilon$ . This value was reduced by nearly 57% when  $\alpha$  was equal to 1.0 (isotropy). One can observe that the performance of repaired and reinforced pavements has a positive correlation with the degree of continuity between the AC overlay and old AC layer. Better pavement performance was observed with better continuity. In addition, the results also indicate that the transversely isotropic characteristics of AC cannot be ignored.

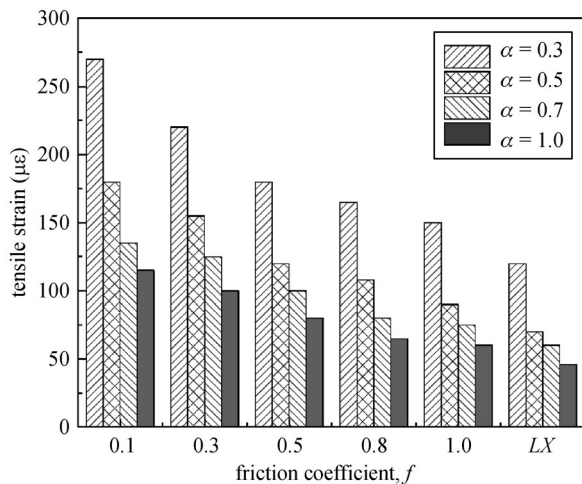


Fig. 12 Horizontal tensile strain at the bottom of the overlay (different interlayer boundary condition)

#### 4.4 Comprehensive analysis for the effects of transverse isotropy

Since the pavement response to the transversely isotropic characteristics of AC plays a very important role in design and analysis, a comparison between the responses to different temperatures under different transversely isotropic conditions were necessary to understand the effect of the modulus gradient of the AC overlay.

Figure 13 shows the peak surface deflection under the different temperatures and the different transversely isotropic conditions. It presents that the properties of the modulus gradient (low temperature, intermediate tempera-

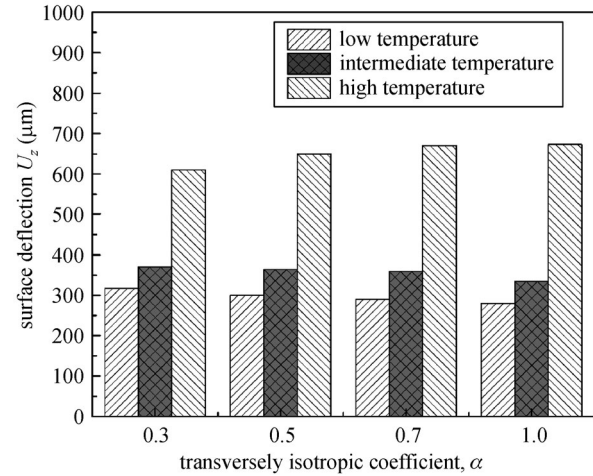


Fig. 13 Maximum surface deflection under different temperature conditions (absolute value)

ture, and high temperature) of AC overlay have significant effects on the peak surface deflection under the same transversely isotropic coefficient,  $\alpha$ . Surface deflection is the largest, considering the high temperature modulus gradient properties of the AC overlay, and the lowest value appeared in the low temperature modulus gradient properties.

In addition, the maximum surface deflection increased under high temperatures, and the maximum surface deflection decreased under low and intermediate temperatures as  $\alpha$  increased. Note that the range in variation was small. There are two groups of road deformation ( $\alpha = 0.3$  and  $\alpha = 1.0$ ) for nephogram of surface deflections corresponding to low temperature, intermediate temperature, and high temperature from Table 2. It also indicates that the transversely isotropic characteristic of the AC overlay had a certain degree of influence on the peak surface deflection, but this influence was small.

Horizontal tensile strain in the bottom of the AC overlay is the key index to control the fatigue cracking of AC overlay. Figure 14 provides the horizontal tensile strain at the bottom of the overlay under different temperatures transversely isotropic conditions. Figure 14 shows that the horizontal tensile strain at the bottom of the AC overlay increased with the decrease in the value of  $\alpha$  under low, intermediate, and high temperatures. It should be noted that the horizontal tensile strain at the bottom of the AC overlay increased more significantly under intermediate and high temperatures. It was shown that the transversely isotropic characteristic of AC is not good for resistance to fatigue cracking. In addition, the horizontal tensile strain at the bottom of the AC overlay was the largest with high temperature modulus gradient, and it was the smallest with low temperature modulus gradient properties of the AC overlay. It was shown that the increase in the modulus of the AC overlay reduced the bottom tensile strain of the

**Table 2** Nephogram of surface deflections under different temperature conditions

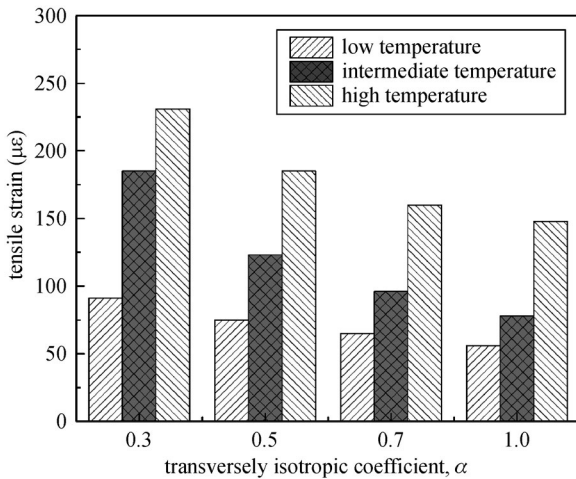
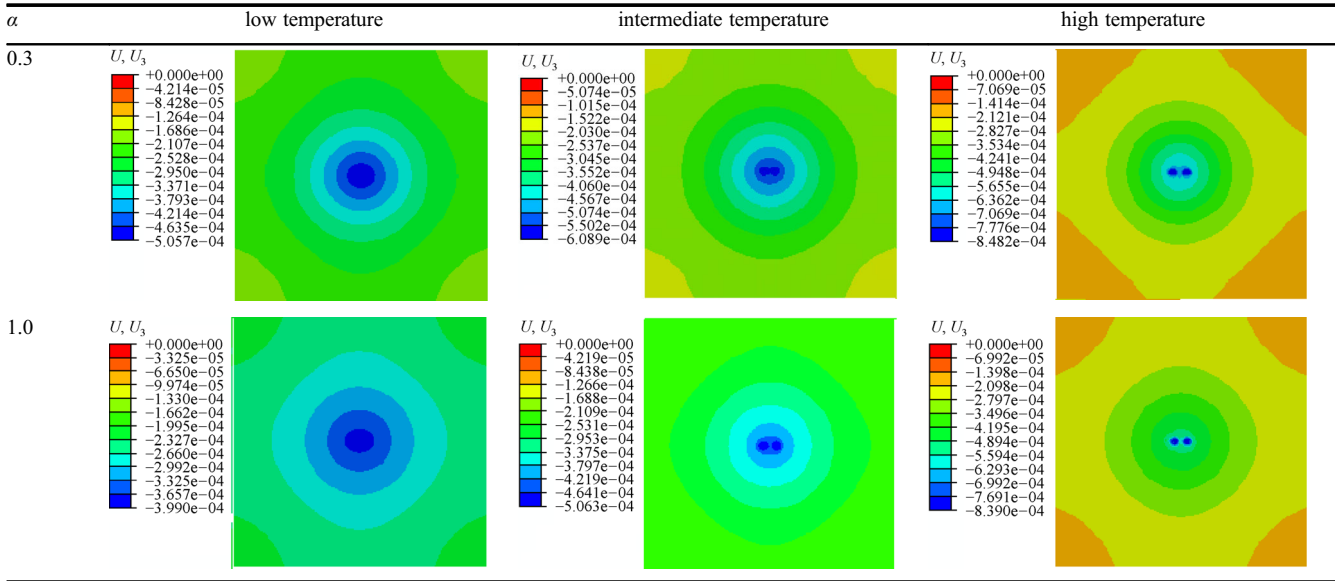


**Fig. 14** Horizontal tensile strain at the bottom of overlay (different temperature conditions)

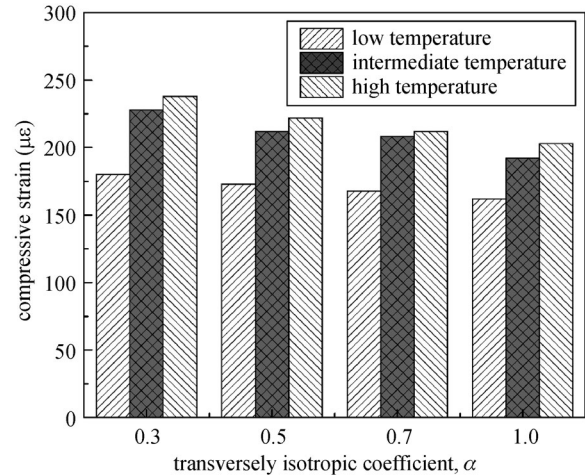


**Fig. 15** Vertical strain at top of subgrade (different temperature conditions)

overlay, which is beneficial to the pavement’s resistance to fatigue cracking.

The compressive strain at the top of the soil foundation is an important index for rutting. It can be seen in Fig. 15 that the compressive strain at the top of the subgrade under low, intermediate, and high temperatures increased with the decrease in the value of  $\alpha$ . The compressive strain under high temperature modulus gradient properties of AC overlay was the largest and the smallest was under low temperature modulus gradient. The following three conclusions are presented here: 1) The transversely isotropic characteristic of AC has a great impact on the compressive strain depending on the overlay material’s temperature modulus properties at the top of subgrade layer; 2) the anti-rutting ability of pavement is lower than that of traditional

pavement when considering the transversely isotropic characteristic of AC; and 3) appropriately increasing the modulus of AC overlay can reduce the compressive strain at the top of the subgrade layer, thus prolonging the rutting of pavement.

## 5 Uncertainty and sensitivity analysis

The uncertainty input parameters inherently create variation in the finite element modeling (FEM) model output. SA is the study of how much the FEM model output is affected by changes in the input parameters [14,15,55–57]. The objective of SA in this paper is to quantitatively assess the effect of uncertain parameter, i.e., transversely isotropic

coefficients, on the mechanical behavior of AC overlay, i.e., the surface deflection, shear strain, and shear stress of AC overlay. In this section, the definition of the parameters and their types, mean, and standard deviation are summarized in Tables 3 and 4.

The uncertainty in the FEM model input parameters inherently creates variation in the model output. Quantifying such variation requires the determination of standard deviation of the model output, as shown in Tables 3 and 4. In addition, the standardized regression coefficients (SRC) is an SA method which is based on the linear regression analysis. The output,  $\mathbf{R} = f(I_1, I_2, \dots, I_n)$ , is computed by the FEM model for the input parameters  $\mathbf{I} = (I_1, I_2, \dots, I_n)$ . Once the regression coefficient  $a_i$  is computed for  $i$ -th input parameter,  $I_i$ , the value of  $SRC_i$  could be calculated as [14]:

$$SRC_i = a_i b_i / c_r, \quad (5)$$

where  $b_i$  and  $c_r$  are the standard deviations of  $I_i$  and  $\mathbf{R}$ ,

respectively. Note that the bigger value of SRC, the more sensitive of the FEM model with respect to the input parameter  $I$ .

According to Section 4, transversely isotropic coefficients have different degrees of influence on different outputs, i.e., the surface deflection, shear strain, and shear stress of AC overlay. In this section, the SA of the outputs affected by the change of transversely isotropic coefficients is achieved. Figure 16 depicts the sensitivity indices based on SRCs method. Figure 16(a) demonstrates the sensitivity indices of the effects of transversely isotropic coefficient on the maximum surface deflection, maximum shear stress, and maximum shear strain of AC overlay at low temperature condition—The SRC values are 0.0139, 0.0449, and 0.00288, respectively. Figure 16(b) shows the sensitivity indices of the effects of transversely isotropic coefficient affecting on the maximum surface deflection, maximum shear stress, and maximum shear

**Table 3** Statistical properties of input parameters and outputs at low temperature condition

parameter definition (unit)	types	mean	standard deviation
transversely isotropic coefficient $\alpha$	input	0.625	0.2986
Max. surface deflection $U_z$ ( $\mu\text{m}$ )	output	-303.70	9.7885
Max. shear stress $\sigma$ (kPa)	output	144.45	4.5092
Max. shear strain $\varepsilon$ ( $\mu\epsilon$ )	output	933.75	29.1401

**Table 4** Statistical properties of input parameters and outputs at high temperature condition

parameter definition (unit)	types	mean	standard deviation
transversely isotropic coefficient $\alpha$	input	0.625	0.2986
Max. surface deflection $U_z$ ( $\mu\text{m}$ )	output	-647.75	19.2922
Max. shear stress $\sigma$ (kPa)	output	119.5	6.5383
Max. shear strain $\varepsilon$ ( $\mu\epsilon$ )	output	927.5	102.3196

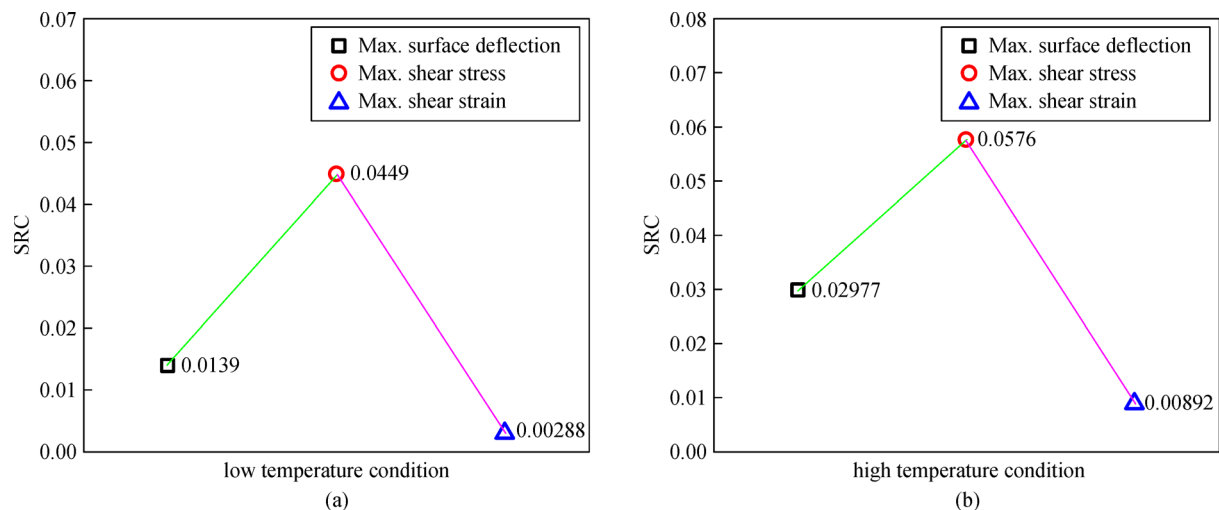


**Fig. 16** Sensitivity analysis of the effect of anisotropic coefficients on AC overlay mechanical behaviors, i.e., Max. surface deflection, shear stress, and shear strain. (a) Low temperature condition; (b) high temperature condition

strain of AC overlay at high temperature condition—the *SRC* value are 0.02977, 0.0576, and 0.00892, respectively. We can see from these *SRC* values that the maximum shear stress in the AC overlay is the most important output parameter affected by the transversely isotropic coefficients at low and high temperature conditions.

## 6 Conclusions

When analytically comparing the mechanical behavior of the transversely isotropic and isotropic model under a constant static load, differences are seen in terms of deflection, strain, and stress. In addition, the SA method was also used to study how much the mechanical behaviors of AC overlay are affected by changes in the model input parameter, i.e., transversely isotropic coefficients. Based on the preceding models, one can draw the following conclusions:

1) It was found that the transversely isotropic characteristic of AC had no obvious effect on the surface deflection of the AC overlay pavement. However, the transversely isotropic characteristic of AC has a larger influence on the shear stress and shear strain of the overlay in comparison to its deflection. All of these features increased with decreases in the transversely isotropic coefficient,  $\alpha$ , of AC.

2) The mechanical behavior was more obvious when the modulus gradient properties of the AC overlay, determined by temperature, were considered. Under low temperature conditions, the mechanical behavior was less obvious in comparison to intermediate and high temperatures.

3) There was a positive correlation between pavement performance and the bonding state of the boundary between the AC overlay and old AC layer. In other words, pavement performance improved with continuity between the layers.

4) The maximum shear stress in the AC overlay was the most significant output parameter affected by the transversely isotropic coefficients.

5) The above facts have important implications for the repair and reinforcement of existing pavements. Current studies that use isotropic elasticity analysis may underestimate the mechanical behaviors of the pavement.

## References

- Dave E V, Buttlar W G. Thermal reflective cracking of asphalt concrete overlays. *International Journal of Pavement Engineering*, 2010, 11(6): 477–488
- Dempsey B. Development and performance of interlayer stress-absorbing composite in asphalt concrete overlays. *Transportation Research Record: Journal of the Transportation Research Board*, 2002, 1809: 175–183
- Khodaii A, Fallah S, Moghadas Nejad F. Effects of geosynthetics on reduction of reflection cracking in asphalt overlays. *Geotextiles and Geomembranes*, 2009, 27(1): 1–8
- Wang Y. The effects of using reclaimed asphalt pavements (RAP) on the long-term performance of asphalt concrete overlays. *Construction & Building Materials*, 2016, 120: 335–348
- Kuo C M, Hsu T R. Traffic induced reflective cracking on pavements with geogrid-reinforced asphalt concrete overlay. In: *Proceedings of the 82th Annual Meeting at the Transportation Research Board (CD-ROM)*. 2003
- Miller S, Hartmann T, Dorée A. Measuring and visualizing hot mix asphalt concrete paving operations. *Automation in Construction*, 2011, 20(4): 474–481
- Adu-Osei A, Little D, Lytton R. Cross-anisotropic characterization of unbound granular materials. *Transportation Research Record: Journal of the Transportation Research Board*, 2001, 1757: 82–91
- Kim S H, Little D, Masad E. Simple methods to estimate inherent and stress-induced anisotropy of aggregate base. *Transportation Research Record: Journal of the Transportation Research Board*, 2005, 1913: 24–31
- Wang L, Hoyos L R, Wang J, Voyiadjis G, Abadie C. Anisotropic properties of asphalt concrete: Characterization and implications for pavement design and analysis. *Journal of Materials in Civil Engineering*, 2005, 17(5): 535–543
- Yan K, Xu H, You L. Analytical layer-element approach for wave propagation of transversely isotropic pavement. *International Journal of Pavement Engineering*, 2016, 17(3): 275–282
- Masad S, Little D, Masad E. Analysis of flexible pavement response and performance using isotropic and anisotropic material properties. *Journal of Transportation Engineering*, 2006, 132(4): 342–349
- Oh J H, Lytton R, Fernando E. Modeling of pavement response using nonlinear cross-anisotropy approach. *Journal of Transportation Engineering*, 2006, 132(6): 458–468
- Mao Y, Robertson J M, Mu X, Mather P T, Qi H J. Thermoviscoplastic behaviors of anisotropic shape memory elastomeric composites for cold programmed non-affine shape change. *Journal of the Mechanics and Physics of Solids*, 2015, 85: 219–244
- Hamdia K M, Msekh M A, Silani M, Vu-Bac N, Zhuang X, Nguyen-Thoi T, Rabczuk T. Uncertainty quantification of the fracture properties of polymeric nanocomposites based on phase field modeling. *Composite Structures*, 2015, 133: 1177–1190
- Vu-Bac N, Rafiee R, Zhuang X, Lahmer T, Rabczuk T. Uncertainty quantification for multiscale modeling of polymer nanocomposites with correlated parameters. *Composites. Part B, Engineering*, 2015, 68: 446–464
- Hamdia K M, Silani M, Zhuang X, et al. Stochastic analysis of the fracture toughness of polymeric nanoparticle composites using polynomial chaos expansions. *International Journal of Fracture*, 2017, 206(2): 215–227
- Hamdia K M, Silani M, Zhuang X, He P, Rabczuk T. Stochastic predictions of bulk properties of amorphous polyethylene based on molecular dynamics simulations. *Mechanics of Materials*, 2014, 68: 70–84
- Nazarian S, Alvarado G. Impact of temperature gradient on modulus of asphaltic concrete layers. *Journal of Materials in Civil Engineering*, 2006, 18(4): 492–499

19. Arulrajah A, Disfani M M, Horpibulsuk S, Suksiripattanapong C, Prongmanee N. Physical properties and shear strength responses of recycled construction and demolition materials in unbound pavement base/subbase applications. *Construction & Building Materials*, 2014, 58: 245–257
20. Pasetto M, Baldo N. Experimental evaluation of high performance base course and road base asphalt concrete with electric arc furnace steel slags. *Journal of Hazardous Materials*, 2010, 181(1–3): 938–948
21. Ozer H, Al-Qadi I L, Wang H, Leng Z. Characterisation of interface bonding between hot-mix asphalt overlay and concrete pavements: Modelling and *in-situ* response to accelerated loading. *International Journal of Pavement Engineering*, 2012, 13(2): 181–196
22. Guo C, Wang F, Zhong Y. Assessing pavement interfacial bonding condition. *Construction & Building Materials*, 2016, 124: 85–94
23. Feng Y, Okamoto R J, Namani R, Genin G M, Bayly P V. Measurements of mechanical anisotropy in brain tissue and implications for transversely isotropic material models of white matter. *Journal of the Mechanical Behavior of Biomedical Materials*, 2013, 23: 117–132
24. Sone H, Zoback M D. Mechanical properties of shale-gas reservoir rocks—Part 1: Static and dynamic elastic properties and anisotropy. *Geophysics*, 2013, 78(5): D381–D392
25. Masad E, Tashman L, Samedavan N, Little D. Micromechanics-based analysis of stiffness anisotropy in asphalt mixtures. *Journal of Materials in Civil Engineering*, 2002, 14(5): 374–383
26. Motola Y, Uzan J. Anisotropy of field-compacted asphalt concrete material. *Journal of Testing and Evaluation*, 2007, 35(1): 103–105
27. Ju D. Anisotropy of asphalt concrete and the influence in pavement. Dissertation for the Doctoral Degree. Nanjing: Southeast University, 2011 (in Chinese)
28. Zhang Q J, Huang Z Y, Liu Z. Analysis of gradient modulus of asphalt pavements. *Low Temperature Architecture Technology*, 2011, 33: 48–50 (in Chinese)
29. Buttlar W G, Paulino G H, Song S H. Application of graded finite elements for asphalt pavements. *Journal of Engineering Mechanics*, 2006, 132(3): 240–249
30. Li F, Sun L, Fang J. Pavement structure shear stress analysis considering stiffness gradients of asphalt course. *Transportation Science and Technology*, 2005, (4): 1–3 (in Chinese)
31. Mu F, Vandenbossche J. Establishing effective linear temperature gradients for ultrathin bonded concrete overlays on asphalt pavements. *Transportation Research Record: Journal of the Transportation Research Board*, 2012, 2305: 24–31
32. Shen J A. *Road Performance of Asphalt and Asphalt Mixture*. Beijing: China Communications Press, 2001 (in Chinese)
33. Rushing J F, Little D N. Static creep and repeated load as rutting performance tests for airport HMA mix design. *Journal of Materials in Civil Engineering*, 2014, 26(9): 04014055
34. Rushing J F, Little D N, Garg N. Selecting a rutting performance test for airport asphalt mixture design. *Road Materials and Pavement Design*, 2014, 15(Suppl 1): 172–194
35. Rushing J F, Little D N. Creep and repeated creep-recovery as rutting performance tests for airport HMA mix design. In: *Proceedings of Transportation Research Board 2013 Annual Meeting*. Washington, 2013
36. Sun L. *Structural Behavior Theory of Asphalt Pavements*. Beijing: China Communications Press, 2005 (in Chinese)
37. You L, Yan K, Hu Y, Zollinger D G. Spectral element solution for transversely isotropic elastic multi-layered structures subjected to axisymmetric loading. *Computers and Geotechnics*, 2016, 72: 67–73
38. Armero F, Kim J. Three-dimensional finite elements with embedded strong discontinuities to model material failure in the infinitesimal range. *International Journal for Numerical Methods in Engineering*, 2012, 91(12): 1291–1330
39. Mahmoud E, Saadeh S, Hakimelahi H, Harvey J. Extended finite-element modelling of asphalt mixtures fracture properties using the semi-circular bending test. *Road Materials and Pavement Design*, 2014, 15(1): 153–166
40. Jiang G, Li J, Tang G. A modeling method of the bolted joint structure and analysis of its stiffness characteristics. In: Lei F, Xu Q, Zhang G, eds. *Machinery, Materials Science and Engineering Applications*. Boca Raton: CRC Press/Balkema, 2016, 229–236
41. de Melo V V, Carosio G L C. Evaluating differential evolution with penalty function to solve constrained engineering problems. *Expert Systems with Applications*, 2012, 39(9): 7860–7863
42. Albrecher H, Cheung E C, Thonhauser S. Randomized observation periods for the compound Poisson risk model: The discounted penalty function. *Scandinavian Actuarial Journal*, 2013, 2013(6): 424–452
43. Ryzhii V, Satou A, Otsuji T, Ryzhii M, Mitin V, Shur M S. Dynamic effects in double graphene-layer structures with inter-layer resonant-tunnelling negative conductivity. *Journal of Physics. D, Applied Physics*, 2013, 46(31): 315107
44. de Beer M, Maina J, Netterberg F. Mechanistic modelling of weak interlayers in flexible and semi-flexible road pavements: Part 2. *Journal of the South African Institution of Civil Engineering*, 2012, 54(1): 43–54
45. Canestrari F, Ferrotti G, Lu X, Millien A, Partl M N, Petit C, Phelipot-Mardel e A, Piber H, Raab C. Mechanical testing of interlayer bonding in asphalt pavements. In: Partl M N, Bahia H U, Canestrari F, de la Roche C, Di Benedetto H, Piber H, Sybilski D, eds. *Advances in Interlaboratory Testing and Evaluation of Bituminous Materials*. Dordrecht: Springer, 2013, 303–360
46. Mhanna M, Sadek M, Shahrour I. Numerical modeling of traffic-induced ground vibration. *Computers and Geotechnics*, 2012, 39: 116–123
47. Xia K, Yang Y. Three-dimensional finite element modeling of tire/ground interaction. *International Journal for Numerical and Analytical Methods in Geomechanics*, 2012, 36(4): 498–516
48. Hu C, Ma J, Yu Y, Luo Y. Optimal design on dowel length for cement concrete pavement. *International Journal of Pavement Research and Technology*, 2016, 9(6): 414–423
49. Thakur J K, Han J, Pokharel S K, Parsons R L. Performance of geocell-reinforced recycled asphalt pavement (RAP) bases over weak subgrade under cyclic plate loading. *Geotextiles and Geomembranes*, 2012, 35: 14–24
50. Khavassefat P, Jelagin D, Birgisson B. A computational framework for viscoelastic analysis of flexible pavements under moving loads. *Materials and Structures*, 2012, 45(11): 1655–1671
51. You L, Yan K, Hu Y, Liu J, Ge D. Spectral element method for

- dynamic response of transversely isotropic asphalt pavement under impact load. *Road Materials and Pavement Design*, 2018, 19(1): 223–238
52. Gajewski J, Sadowski T. Sensitivity analysis of crack propagation in pavement bituminous layered structures using a hybrid system integrating artificial neural networks and finite element method. *Computational Materials Science*, 2014, 82: 114–117
53. Lee J W, Lee M G, Barlat F. Finite element modeling using homogeneous anisotropic hardening and application to spring-back prediction. *International Journal of Plasticity*, 2012, 29: 13–41
54. Kim S K, Lee C S, Kim J H, Kim M H, Lee J M. Computational evaluation of resistance of fracture capacity for SUS304L of liquefied natural gas insulation system under cryogenic temperatures using ABAQUS user-defined material subroutine. *Materials & Design*, 2013, 50: 522–532
55. Vu-Bac N, Lahmer T, Zhang Y, Zhuang X, Rabczuk T. Stochastic predictions of interfacial characteristic of polymeric nanocomposites (PNCs). *Composites. Part B, Engineering*, 2014, 59: 80–95
56. Vu-Bac N, Silani M, Lahmer T, Zhuang X, Rabczuk T. A unified framework for stochastic predictions of mechanical properties of polymeric nanocomposites. *Computational Materials Science*, 2015, 96: 520–535
57. Vu-Bac N, Lahmer T, Zhuang X, Nguyen-Thoi T, Rabczuk T. A software framework for probabilistic sensitivity analysis for computationally expensive models. *Advances in Engineering Software*, 2016, 100: 19–31